

# Fluorescence probe of polypeptide conformational dynamics in gas phase and in solution

Anthony T. Iavarone, Jan Meinen<sup>1</sup>, Susanne Schulze<sup>1</sup>, Joel H. Parks\*

*The Rowland Institute at Harvard, 100 Edwin H. Land Blvd., Cambridge, MA 02142, United States*

Received 28 September 2005; received in revised form 30 November 2005; accepted 30 November 2005

## Abstract

Fluorescence measurements of polypeptides derivatized with the fluorescent dye BODIPY TMR have been used to probe the polypeptide conformational dynamics as a function of temperature and charge state. Measurements of (BODIPY TMR)-[Pro]<sub>n</sub>-Arg-Trp and (BODIPY TMR)-[Gly-Ser]<sub>m</sub>-Arg-Trp have been performed for charge states 1+ and 2+ of  $n=4$  and 10 and  $m=2$  and 5. The 2+ charge states of both of these polypeptides exhibit similar temperature dependences for equal chain lengths ( $n=4$ ,  $m=2$  and  $n=10$ ,  $m=5$ ) and suggest conformations dominated by Coulomb repulsion. In the absence of such Coulomb repulsion, the 1+ charge state conformations appear to be characterized by the flexibility of the polypeptide chain for which  $[\text{Gly-Ser}]_m > [\text{Pro}]_n$ . Comparisons of these gas phase polypeptide measurements with corresponding measurements in solution provide a direct measure of the effects of solvent on the conformational dynamics. The change in fluorescence as a function of temperature in the gas phase is two orders of magnitude greater than that in solution, a dramatic result we attribute to the restrictions on intramolecular dynamics imposed by diffusion-limited kinetics and the lack of shielding by solvent. Measurements were also made of unsolvated Pro<sub>n</sub> peptides without the tryptophan (Trp) residue to isolate the interaction of the fluorescent dye with charges.

© 2005 Elsevier B.V. All rights reserved.

**Keywords:** Fluorescence; Peptide; Conformation; Dynamics; Proline

## 1. Introduction

Measurements of proteins in the gas phase, when compared with measurements made in solution, can provide deep insight into the effects of the solvent environment on the native molecular structure and dynamics. The conformations of unsolvated protein and peptide ions have been probed using a wide variety of techniques including ion mobility measurements [1–4], ion-molecule [5–7] and dissociation [8–11] reactions, and infrared spectroscopy [12]. We recently demonstrated the measurement of conformational change occurring with increased temperature in unsolvated Trp-cage protein using fluorescence [13]. This novel experiment relies on fluorescence quenching by intramolecular collisions between a fluorescent dye linked to the C-terminus and a tryptophan (Trp) residue to follow the local

changes in the Trp environment occurring during the unfolding. Similar collision processes have been well-established as a probe of conformational change in solution [14–22] but have not previously been studied in gas phase. Consequently, there is a lack of detailed knowledge about the specificity and sensitivity with which such dye–Trp collisions probe local structural changes and about what additional interactions must be taken into account.

Here, we present fluorescence measurements of unsolvated polypeptides ( $\leq 12$  residues) judiciously selected to isolate the details of the quenching process. Polypeptides offer the possibility to study the dependence of the collision process on temperature, chain length and charge state independent of protein tertiary structure effects. As a result, the intramolecular collisions probe structural dynamics arising from temperature-induced flexibility of the polypeptide, repulsive Coulomb interactions and the solvation of charges by the backbone. Analogous measurements in solution are also presented for comparison with the gas phase data. These experiments not only serve to characterize the collision processes but also provide the basis for extending the application of these fluorescence methods to analyses of confor-

\* Corresponding author. Tel.: +1 617 497 4653; fax: +1 617 497 4627.

E-mail address: [parks@rowland.harvard.edu](mailto:parks@rowland.harvard.edu) (J.H. Parks).

<sup>1</sup> Present address: Technische Universität Ilmenau, Institut für Physik, Postfach 10 05 65, 98684 Ilmenau, Germany.

mational change in protein secondary structural elements and non-covalent complexes.

## 2. Experimental

### 2.1. Materials

Peptides labeled with fluorescent dyes were synthesized by BioMer Technology (Concord, CA) and purified by reversed-phase HPLC to a stated purity of >70% prior to shipment. The BODIPY<sup>®</sup> analog of tetramethylrhodamine, BODIPY TMR, was obtained from Molecular Probes (Eugene, OR). The molecular structure and excitation and emission spectra of this dye have been published elsewhere [23,24]. Heating solutions of BODIPY TMR from 293 to 332 K results in a ~10–20% change in the fluorescence emission intensity [24]. The peptide sequences are (BODIPY TMR)-(P)<sub>n</sub>RW (*n* = 4 and 10, referred to herein as “Pro<sub>4</sub>” and “Pro<sub>10</sub>”), (BODIPY TMR)-(P)<sub>n</sub>R (*n* = 4 and 10, “Pro<sub>4</sub> sans Trp” and “Pro<sub>10</sub> sans Trp”) and (BODIPY TMR)-(GS)<sub>m</sub>RW (*m* = 2 and 5, “(GlySer)<sub>2</sub>” and “(GlySer)<sub>5</sub>”). The dye is attached to the peptides via an aminohexanoate linker and the C-termini of the peptides are amidated. Peptide chemical structures are shown in Fig. 1. Acetonitrile (>99.9%) and distilled, deionized water were obtained from Fisher Scientific (Fair Lawn, NJ) and VWR (West Chester, PA), respectively. Electrospray solutions of the peptides are 10<sup>-5</sup> M in 50% acetonitrile/50% water.

### 2.2. Mass spectrometry and fluorescence

Experiments are performed on a quadrupole ion trap mass spectrometer that was designed and built in-house [25]. Ions are formed by nanoelectrospray (nanoES) [26] from needles that are pulled from 1.0 mm o.d. to 0.58 mm i.d. borosilicate glass tubes using a micropipette puller (Model P-87, Sutter Instruments, Novato, CA). The pulled nanoES needles have tips with an inner diameter of ~3–5 μm. The electrospray is initiated by applying a potential of ~1 kV to a platinum wire (0.10 mm diameter, Aldrich, Milwaukee, WI) inserted into the nanoES needle to within 2 mm of the tip. A patch clamp holder (WPI Instruments, Sarasota, FL) holds the wire and nanoES needle in place, with the needle tip positioned approximately 3 mm from the sampling aperture of the mass spectrometer. The droplets and ions generated by nanoES are sampled from atmospheric pressure through a 4.3 cm long stainless steel capillary (0.50 mm i.d.) contained in a cylindrical copper block which is maintained at 333 K by cartridge heaters (Watlow, St. Louis, MO). The voltages applied to the source ion optics are adjusted to optimize the abundance of the ion of interest. Ions pass through differential stages of pumping and enter an octupole ion guide through which they are transferred into the quadrupole ion trap. The ions of interest are isolated using a combination of RF ramping and SWIFT ejection. The electrodes of the ion trap and the helium gas inlet are seated in a copper housing that is resistively heated to temperatures as high as ~443 K with a precision of ±1 K. The

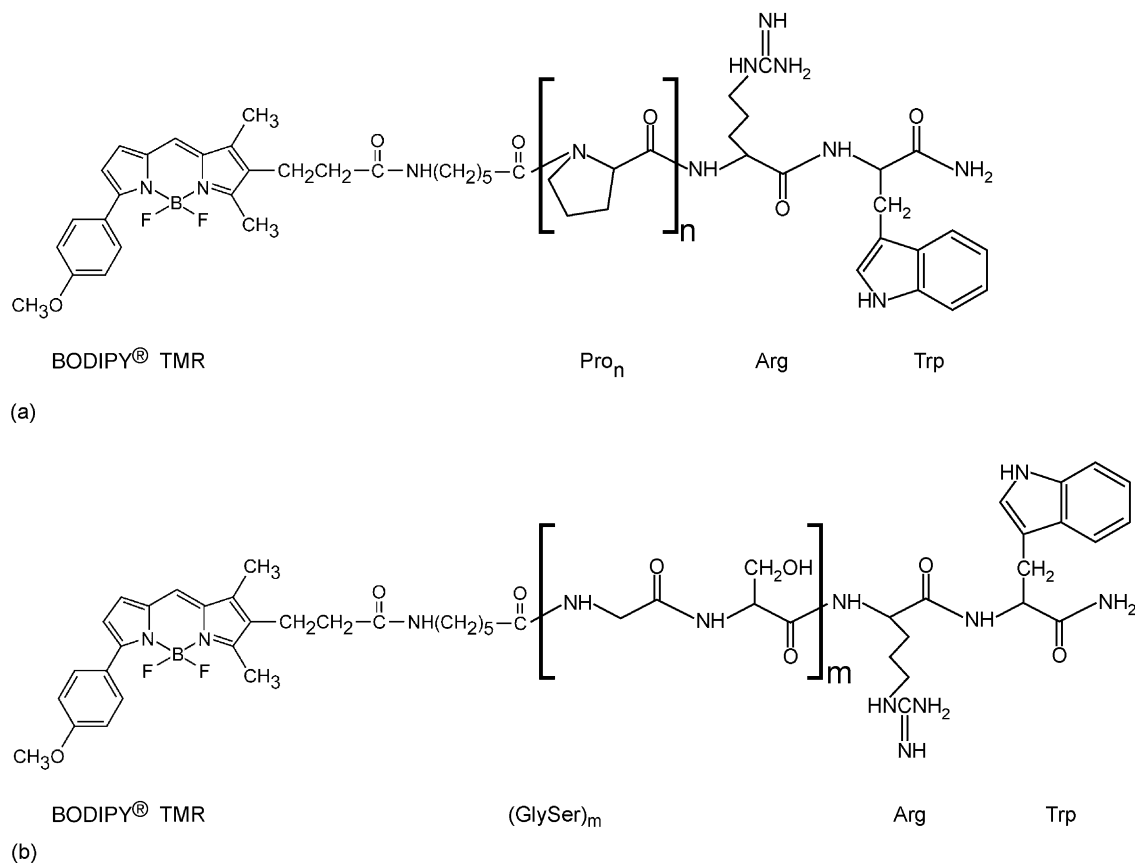


Fig. 1. Chemical structures of (a) (BODIPY TMR)-(P)<sub>n</sub>RW and (b) (BODIPY TMR)-(GS)<sub>m</sub>RW.

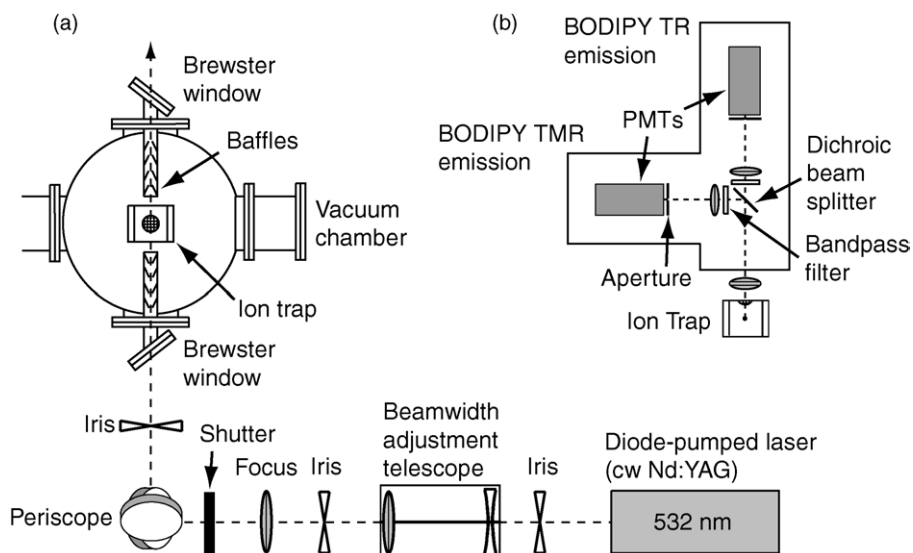


Fig. 2. Diagrams of optics for (a) excitation and (b) detection of fluorescence of trapped gas phase ions.

background helium gas pressure is  $\sim 3 \times 10^{-6}$  Torr and is pulsed to  $\sim 2 \times 10^{-4}$  Torr for ion loading and thermalization. (Independent measurements have shown that the pressure within the ion trap is higher by a factor of  $\sim 30$ – $35$  due to the low conductance of the trap apertures.) Ions are thermalized in the trap for 1 s at  $q_z = 0.50$  before measuring fluorescence. Under these conditions the trapped ions undergo  $>10^5$  collisions which equilibrate the ions with the helium bath gas which is maintained at the temperature of the trap electrodes. No significant loss of ions or any fragmentation are observed on the time frame of these experiments.

Diagrams of the excitation and detection configurations are shown in Fig. 2a and b, respectively. The isolated ions of interest are irradiated with a continuous wave Nd:YAG laser (Millenia VIs, Spectra-Physics, Irvine, CA) for 100 ms at the frequency doubled wavelength of 532 nm and an intensity of  $132 \text{ W/cm}^2$ . The Gaussian laser beam diameter has been decreased to  $\sim 220 \mu\text{m}$  to eliminate scattering of the light on the electrodes and apertures of the trap. The laser–ion interaction volume is  $\sim 10^{-5} \text{ cm}^3$ , or  $\sim 3$ – $15\%$  of the total ion cloud volume, depending on the trap temperature and operating parameters. The overlap between the laser and the ion cloud is optimized by alignment of the laser and by adjustment of the dc bias applied to the endcaps of the trap (the latter alters the position of the ion cloud within the trap). The emitted light is collected through a triplet lens and passes through a bandpass filter to isolate the emission band of BODIPY TMR before impinging on a gallium arsenide photomultiplier (Hamamatsu Photonics, Hamamatsu City, Japan). The emitted light passes through 1 mm apertures before impinging on the photomultipliers, thus limiting the fluorescence collection to a solid angle defined by the laser–ion cloud interaction volume and minimizing the detection of background laser scattering. Zero background detection during the laser excitation pulse is achieved, as demonstrated previously [25]. After the fluorescence measurement, the ions are ejected at  $q_z = 0.908$  and detected by a channel electron mul-

tiplier (K & M Electronics, West Springfield, MA). Twenty-five replicate fluorescence measurements are performed for each data point. Each set of measurements is performed two times on different days and the day-to-day reproducibility is within  $\pm 20\%$ .

### 2.3. Fluorescence spectroscopy

Fluorescence emission and excitation spectra of species in solution are measured on a Model J-810 spectrometer (Jasco, Easton, MD). The excitation wavelength is 540 nm and the excitation and emission bandwidths are both 10 nm. The solutions under study are contained in quartz cuvettes (1 cm pathlength; Spectrocell, Oreland, PA) which are sealed with screw caps to prevent solvent evaporation. The sample temperature is regulated with a precision of  $\pm 0.5 \text{ K}$  by a Peltier effect temperature controller (Model PFD-524S, Jasco). Solutions contain the analyte at  $3 \times 10^{-6} \text{ M}$  in water.

### 2.4. Error analysis

Error bars represent  $\pm$  one standard deviation from the mean unless stated otherwise.

## 3. Results

### 3.1. Peptides in gas phase

The experimental sequence for fluorescence measurements of gas phase peptide ions is illustrated in Fig. 3. Fig. 3a shows the charge state distribution of the peptide Pro<sub>4</sub> formed by nanoES and trapped in the quadrupole ion trap, with the  $(M+H)^+$ ,  $(M+2H)^{2+}$  and  $(M+3H)^{3+}$  ions, denoted herein as 1+, 2+ and 3+, formed at 84, 100 and 19% relative abundance, respectively. The ion of interest, e.g., the 1+, is isolated by ejection of the other ions from the trap (Fig. 3b). The fluorescence of the ion of

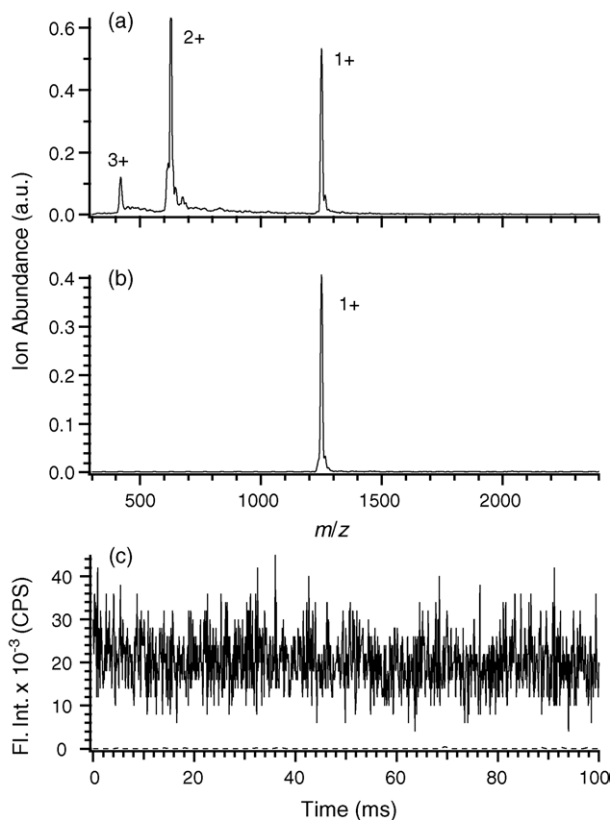


Fig. 3. Experimental sequence for fluorescence measurement of gas phase peptide ions. (a) Charge state distribution of positive ions of the peptide,  $\text{Pro}_4$ , formed by nanoES. Charge states  $(M+H)^+$ ,  $(M+2H)^{2+}$  and  $(M+3H)^{3+}$ , denoted, respectively, as 1+, 2+ and 3+, are formed. (b) Isolation of the 1+ charge state. (c) Fluorescence intensity of the 1+ ion measured over 100 ms (solid line). The average background signal (dotted line) is  $\sim 50$  CPS.

interest is then measured over 100 ms. In this typical example the average signal-to-noise ratio is  $\sim 400$  for  $\sim 200$  ions in the laser interaction volume (Fig. 3c).

### 3.1.1. Relative intensities

Fluorescence measurements were performed at 303, 333, 363, 403 and 438 K for each of the peptide ions of interest. For the 1+ charge state of  $\text{Pro}_4$ , the fluorescence intensity per ion decreases 70% as the temperature is increased from 303 to 438 K (Fig. 4a). The intensity of the  $\text{Pro}_{10}$  1+ at 303 K is 18% lower than that of  $\text{Pro}_4$  1+, however, the difference in intensity of these two ions decreases with increasing temperature and the intensi-

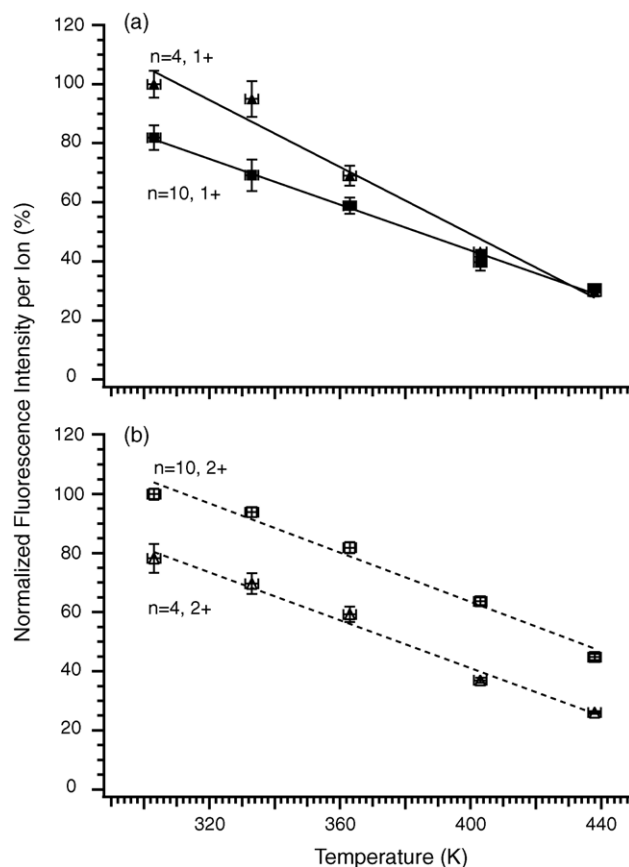


Fig. 4. Normalized fluorescence intensity per ion measured as a function of temperature for the (a) 1+ and (b) 2+ charge states of  $\text{Pro}_n$  for  $n=4$  (triangles) and  $n=10$  (squares), with best-fit lines to the data.

ties converge at the highest temperatures investigated (Fig. 4a). In contrast with the results of the 1+ ions, the intensity of  $\text{Pro}_4$  2+ at 303 K is 22% lower than that of  $\text{Pro}_{10}$  2+, and the intensities of these ions decrease essentially in parallel (by 52 and 55%, respectively) as the temperature is increased to 438 K (Fig. 4b). The intensity of  $(\text{GlySer})_2$  1+ at 303 K is 16% lower than that of  $(\text{GlySer})_5$  1+, and the intensities of these ions decrease 64 and 70%, respectively, as the temperature is increased to 438 K (Fig. 5a). Similarly, the intensity of  $(\text{GlySer})_2$  2+ is 18% lower than that of  $(\text{GlySer})_5$  2+ at 303 K, and the intensities of these ions decrease 62 and 57%, respectively, as the temperature is increased to 438 K (Fig. 5b).

Table 1  
Fluorescence intensities and slopes of intensity vs. temperature of 1+ and 2+ charge states of peptides in gas phase<sup>a</sup>

Peptide	1+ Intensity (CPS/N) <sup>b</sup>	1+ Slope (CPS/N K) <sup>c</sup>	2+ Intensity (CPS/N) <sup>b</sup>	2+ Slope (CPS/N K) <sup>c</sup>
$\text{Pro}_4$	$13.3 \pm 0.9$	$-0.0758 \pm 0.0059$	$6.3 \pm 0.4$	$-0.0328 \pm 0.0022$
$\text{Pro}_4$ sans Trp	$11.0 \pm 0.3$	$-0.0443 \pm 0.0024$	$5.1 \pm 0.1$	$-0.0151 \pm 0.0026$
$\text{Pro}_{10}$	$11.2 \pm 1.0$	$-0.0531 \pm 0.0043$	$8.1 \pm 0.1$	$-0.0337 \pm 0.0027$
$\text{Pro}_{10}$ sans Trp	$10.3 \pm 0.3$	$-0.0398 \pm 0.0021$	$8.1 \pm 0.2$	$-0.0288 \pm 0.0017$
$(\text{GlySer})_2$	$10.3 \pm 0.3$	$-0.0582 \pm 0.0020$	$3.7 \pm 0.1$	$-0.0219 \pm 0.0015$
$(\text{GlySer})_5$	$12.3 \pm 0.3$	$-0.0638 \pm 0.0029$	$4.5 \pm 0.1$	$-0.0184 \pm 0.0015$

<sup>a</sup> Stated errors are  $\pm$  one standard deviation from the mean.

<sup>b</sup> At 303 K.

<sup>c</sup> Slope of the best-fit line.

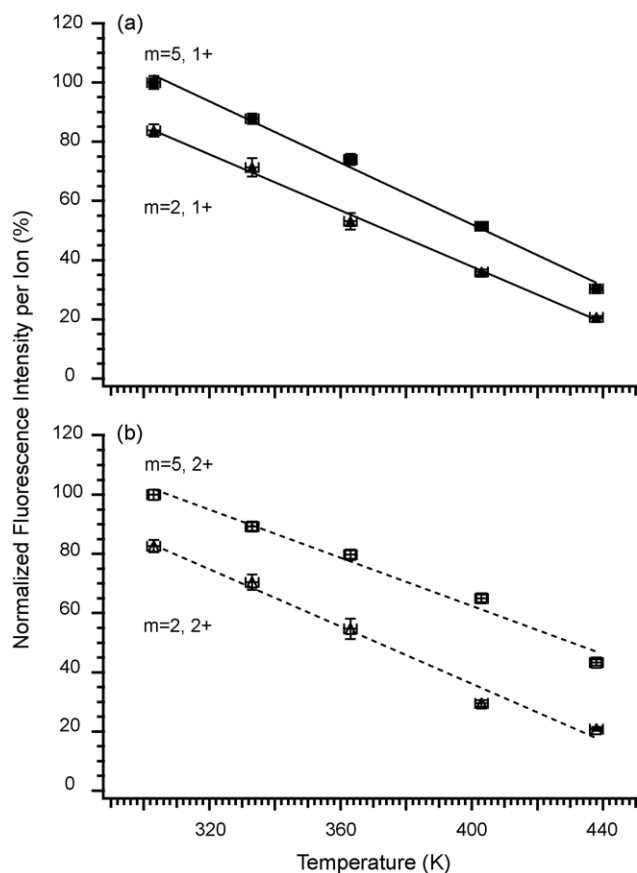


Fig. 5. Normalized fluorescence intensity per ion measured as a function of temperature for the (a) 1+ and (b) 2+ charge states of  $(\text{GlySer})_m$  for  $m=2$  (triangles) and  $m=5$  (squares), with best-fit lines to the data.

### 3.1.2. Absolute intensities

For the ions of  $\text{Pro}_4$  and  $\text{Pro}_{10}$  the absolute fluorescence intensities at 303 K decrease in the order  $\text{Pro}_4$  1+ >  $\text{Pro}_{10}$  1+ >  $\text{Pro}_{10}$  2+ >  $\text{Pro}_4$  2+ (Fig. 6). As the temperature is increased the intensities of  $\text{Pro}_4$  1+,  $\text{Pro}_{10}$  1+ and  $\text{Pro}_{10}$  2+ converge to yield the order of intensities  $\text{Pro}_4$  1+  $\approx$   $\text{Pro}_{10}$  1+  $\approx$   $\text{Pro}_{10}$  2+ >  $\text{Pro}_4$  2+ at

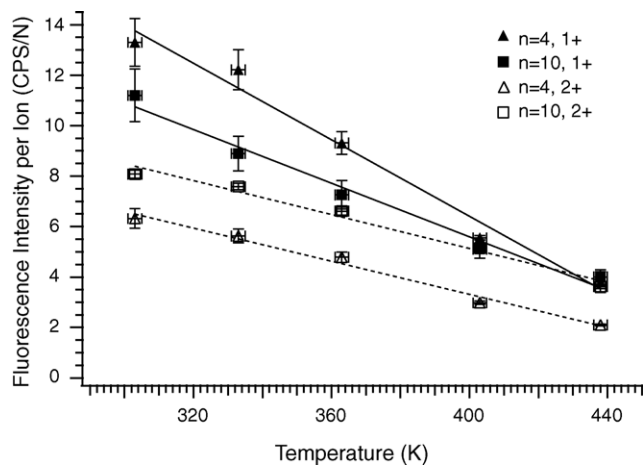


Fig. 6. Absolute fluorescence intensity per ion measured as a function of temperature for the 1+ and 2+ charge states of  $\text{Pro}_n$ ,  $n=4$  and 10, with the best-fit lines to the data.

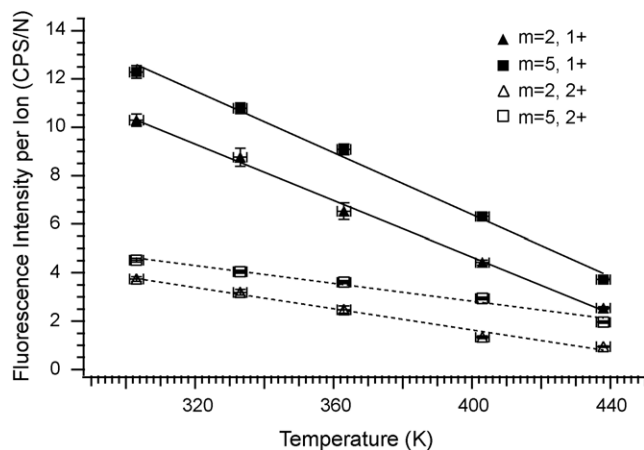


Fig. 7. Absolute fluorescence intensity per ion measured as a function of temperature for the 1+ and 2+ charge states of  $(\text{GlySer})_m$ ,  $m=2$  and 5, with best-fit lines to the data.

438 K (Fig. 6). For  $\text{Pro}_4$  and  $\text{Pro}_{10}$ , the intensity of the 2+ ion at 303 K is 53 and 28% lower, respectively, than that of the 1+ ion, and the rate of decrease in intensity with increasing temperature for the 1+ ion is 131 and 58% larger, respectively, than that of the 2+ ion (Table 1). For the ions of  $(\text{GlySer})_2$  and  $(\text{GlySer})_5$  the absolute fluorescence intensities decrease in the order  $(\text{GlySer})_5$  1+ >  $(\text{GlySer})_2$  1+ >  $(\text{GlySer})_5$  2+ >  $(\text{GlySer})_2$  2+ for all temperatures investigated (Fig. 7). For  $(\text{GlySer})_2$  and  $(\text{GlySer})_5$ , the intensity of the 2+ ion at 303 K is 64 and 63% lower, respectively, than that of the 1+ ion, and the rate of decrease in intensity with increasing temperature for the 1+ ion is 168 and 247% larger, respectively, than that of the 2+ ion (Table 1). From these data it is apparent that (1) fluorescence intensity decreases with increasing temperature, (2) for a given peptide, the 2+ charge state exhibits a lower fluorescence intensity than the 1+ charge state, (3) for a given peptide, the fluorescence intensity of the 1+ charge state decreases more rapidly with increasing temperature than that of the 2+ charge state and (4) for a given charge state and temperature, a higher fluorescence intensity is obtained with the longer polypeptide chain with the notable exception of the 1+ ions of  $\text{Pro}_4$  and  $\text{Pro}_{10}$  (Fig. 4a).

### 3.2. Peptides in solution

Measurements of fluorescence as a function of temperature were also performed in solution for comparison with the measurements in gas phase. For  $\text{Pro}_4$  and  $\text{Pro}_{10}$ , the fluorescence intensity decreases 30 and 10%, respectively, as the temperature is increased from 275 to 343 K (Fig. 8a). For  $(\text{GlySer})_2$  and  $(\text{GlySer})_5$ , the fluorescence intensity decreases 55 and 30%, respectively, over the same temperature range (Fig. 8b).

### 3.3. Peptides sans Trp

Experiments were also performed in gas phase using  $\text{Pro}_n$  peptides that lack the C-terminal Trp residue to remove the possibility for collisional quenching of BODIPY TMR fluorescence by Trp. In contrast to the results obtained with  $\text{Pro}_4$  and  $\text{Pro}_{10}$ ,

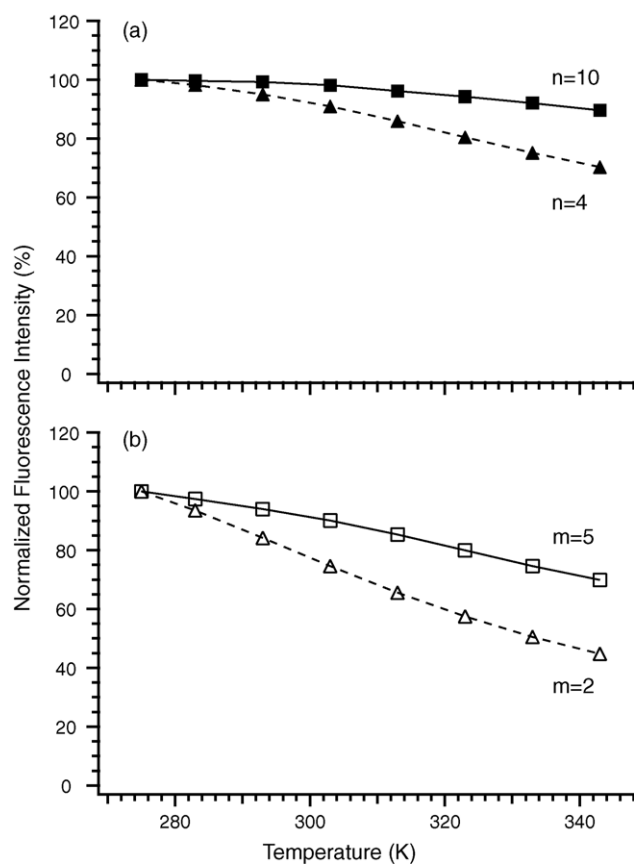


Fig. 8. Normalized fluorescence intensity of (a) Pro<sub>n</sub> for  $n=4$  and  $10$  (represented by closed triangles and squares, respectively) and (b) (GlySer)<sub>m</sub> for  $m=2$  and  $5$  (open triangles and squares, respectively) measured in aqueous solution ( $3 \times 10^{-6}$  M) as a function of temperature. The lines connecting the markers are included to guide the eye.

the fluorescence intensities measured for 1+ ions of Pro<sub>4</sub> sans Trp are very similar to those of Pro<sub>10</sub> sans Trp at all temperatures investigated, and the intensities of the 1+ ions of both Pro<sub>4</sub> sans Trp and Pro<sub>10</sub> sans Trp decrease 55% as the temperature is increased from 303 to 438 K (Fig. 9a). For the 2+ ions the intensity of Pro<sub>4</sub> sans Trp at 303 K is 37% lower than that of Pro<sub>10</sub> sans Trp, and the intensities of these ions decrease 24 and 47%, respectively, as the temperature is increased to 438 K (Fig. 9b). The absolute fluorescence intensities decrease in the order Pro<sub>4</sub> sans Trp 1+  $\approx$  Pro<sub>10</sub> sans Trp 1+ > Pro<sub>10</sub> sans Trp 2+ > Pro<sub>4</sub> sans Trp 2+ (Fig. 10). For Pro<sub>4</sub> sans Trp and Pro<sub>10</sub> sans Trp, the intensity of the 2+ ion at 303 K is 53 and 21% lower, respectively, than that of the 1+ ion, and the rate of decrease in intensity with increasing temperature for the 1+ ion is 193 and 38% larger, respectively, than that of the 2+ ion (Table 1).

#### 4. Discussion

The fluorescence data shown in Section 3 exhibit similar qualitative dependences on temperature, charge state and chain length. For each polypeptide chain an increase in temperature yields a decrease in detected fluorescence, the rate of which depends on charge state and chain length. The higher charge state and shorter chain length produces lower fluorescence inten-

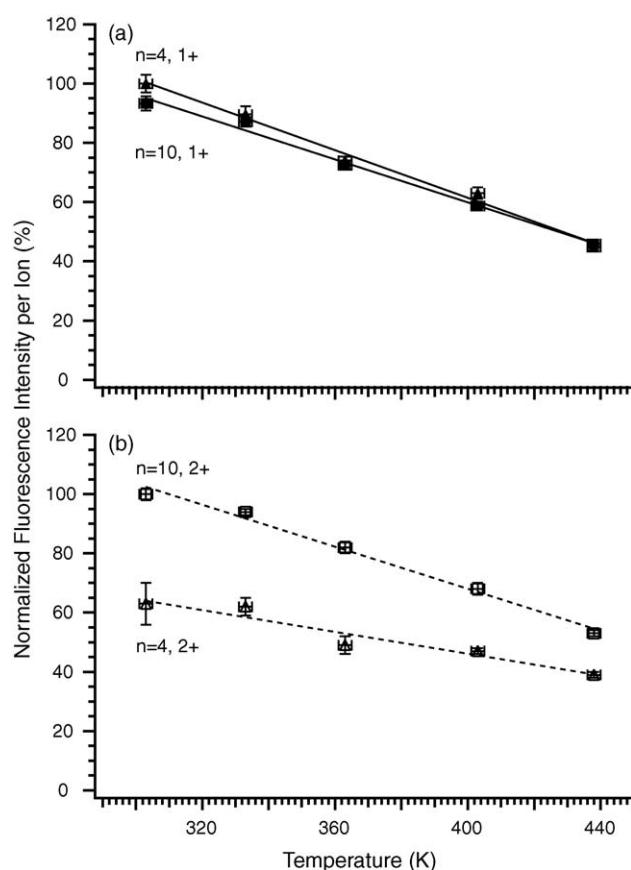


Fig. 9. Normalized fluorescence intensity per ion measured as a function of temperature for the (a) 1+ and (b) 2+ charge states of Pro<sub>n</sub> sans Trp for  $n=4$  (triangles) and  $n=10$  (squares), with best-fit lines to the data.

sities with the single exception of Pro<sub>4</sub> and Pro<sub>10</sub> in the 1+ state. The 2+ charge state always shows a smaller rate of change with temperature than the 1+ charge state. Notwithstanding these commonalities, the absolute slopes and intensities in Table 1 indicate that there are significant quantitative differences. In the following analysis these variations will be correlated with different polypeptide dynamics. The basis for these comparisons

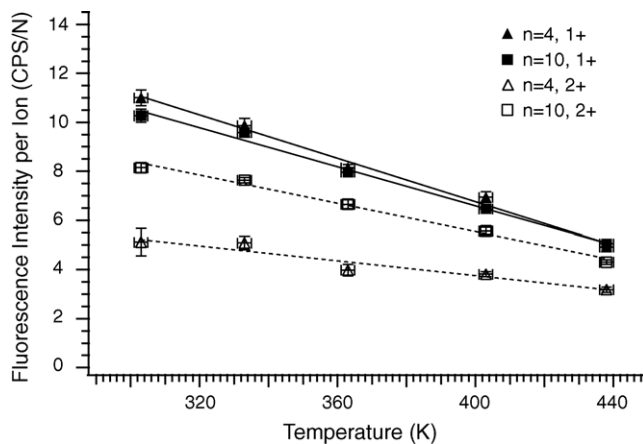


Fig. 10. Absolute fluorescence intensity per ion measured as a function of temperature for the 1+ and 2+ charge states of Pro<sub>n</sub> sans Trp,  $n=4$  or  $10$ , with best-fit lines to the data.

lies in the fact that the fluorescence variations rely on local interactions of the dye with specific areas of the polypeptide chain. These measurements identify two primary processes responsible for changes in dye fluorescence: intramolecular collisions between the dye and the Trp residue and interactions between the dye and charges.

#### 4.1. BODIPY TMR–tryptophan interaction

Previous studies of fluorescence quenching in solution [13,14,17,22] indicate that quenching can occur through contact formation between Trp and the dye (interaction distance  $\sim 5 \text{ \AA}$ ). Here, the requirement for dye–Trp collisions is not that the conformation describe a structural isomer in which the average dye–Trp separation is reduced to  $\leq 5 \text{ \AA}$  but that the *fluctuations* of the dye–Trp separation about the average occur at a sufficient rate to exhibit the observed quenching of the fluorescence. We have performed solution-phase measurements (Meinen et al., in preparation) of both bimolecular and intramolecular quenching of BODIPY TMR fluorescence by Trp. Stern–Volmer analysis of bimolecular quenching indicates that dynamic quenching is approximately twice as efficient as static quenching. The results of fluorescence quenching measurements combined with cyclic voltammetry measurements of the BODIPY TMR redox potential yield convincing evidence for quenching via photoinduced charge transfer (Meinen et al., in preparation; [27–31]). In this process, collisions between Trp and the excited BODIPY TMR form a complex in which an electron is transferred from Trp to the hole in the BODIPY TMR  $S_0$  state. The electron in the excited  $S_1$  state is then back-transferred to Trp thus providing a non-radiative decay channel.

We assume intramolecular interactions will be an especially important quenching mechanism in the gas phase because the dynamic rates will not be constrained by diffusion-limited kinetics as discussed below. In the following discussion we assume that quenching of BODIPY TMR fluorescence by Trp is dominated by formation of a charge transfer complex.

#### 4.2. BODIPY TMR–charge interaction

The interaction of dyes with electrostatic fields has been studied extensively in solution phase [32–34] and the primary effect is to perturb the  $S_0$  and  $S_1$  levels through dipole interactions with the field. The energy separation introduced by the field perturbation is estimated in the two level approximation [33] by

$$E(S_0) - E(S_1) = hc\Delta\nu = (\vec{\mu}_0 - \vec{\mu}_1)\vec{E} = -\Delta\vec{\mu}\vec{E} \quad (1)$$

where  $E$  is the level energy,  $\Delta\nu$  the shift in wave number,  $\Delta\mu$  the differential dipole moment and  $E$  is the electrostatic field. In solution-phase studies, field strengths as high as  $\sim 10^5$  to  $10^6 \text{ V/cm}$  have been measured [33]. Alternatively, it is also possible that the charge–dipole interaction shifts the dye electronic states into resonance with the pump photons to open additional non-radiative relaxation channels [35].

In gas phase measurements, interactions of the tethered BODIPY TMR dye with a charged residue occur in the absence of shielding by solvent. In this case the electric field strengths

can approach  $\sim 5 \times 10^7 \text{ V/cm}$  for collision impact parameters of  $\sim 5 \text{ \AA}$ . The differential dipole moment for BODIPY TMR [36] of  $\Delta\mu = -0.54 \text{ D}$  yields a maximum spectral blue shift of  $\sim 17 \text{ nm}$  at this separation neglecting shielding effects. Even for such large fields, the rotational kinetic energy  $3kT \gg \mu_0 E$  for a dipole moment of  $\mu_0 = 3.3 \text{ D}$  in the ground state [36]. In this case, the dye orientation will fluctuate in the field during the radiative lifetime, and as a result could reduce the average spectral shift.

A significant spectral shift also requires that the dye remain in the presence of the charged residue for a time comparable to the radiative lifetime  $\sim 5 \text{ ns}$  of BODIPY TMR. Consider the interaction potential which combines charge–dipole and charge-induced–dipole interactions

$$V = -\frac{\alpha_0 e^2}{2r^4} - \frac{e\mu_0 \cos\theta}{r^2} \quad (2)$$

Approximating the polarizability of BODIPY TMR by that of anthracene [37],  $\alpha_0 \approx 25 \text{ \AA}^3$ , yields an estimate of the attractive well depth of  $V \approx 1 \text{ eV}$  at the van der Waals separation of  $\sim 4 \text{ \AA}$ . An interaction potential of this strength could maintain a proximity between BODIPY TMR and the charged residue during the radiative lifetime of the dye. Such localization of the dye at the protonated Arg has been observed in preliminary molecular dynamics simulations.

#### 4.3. Polypeptide dynamics

The preceding discussion presented the feasibility of processes leading to fluorescence variations via intramolecular dynamics, the details of which will be further investigated in planned molecular dynamics simulations. These processes form a basis for a probe of polypeptide dynamics which depends on local interactions. The rate of intramolecular collisions between the dye and specific amino acid residues clearly depends on the position of the residue. As a result, the fluorescence measured as a function of temperature can be interpreted in terms of this position which is a function of the polypeptide conformation. Because the charge state is an important factor determining the spectral shifts, Coulomb repulsive forces and charge-induced structural changes, we organize the discussion for the various peptide sequences by charge state.

##### 4.3.1. 1+ Charge state

The overall decrease in fluorescence intensity with increasing temperature follows from the increased fluctuations of the polypeptide backbone and side chains. For the 1+ ions of Pro<sub>4</sub> and Pro<sub>10</sub>, the fluorescence intensity and rate of change with temperature depend on whether Trp is present. For both chain lengths ( $n = 4$  and  $10$ ) the presence of Trp results in higher fluorescence intensities and a larger rate of change with temperature (Table 1). Although the origin for these results is unclear, one possibility is smaller intramolecular collision rates in the peptides containing Trp stemming from larger separations between the dye and the Trp/charge positions. In all 1+ ions the protonated site is the Arg residue adjacent to Trp. The Trp dipole moment in the ground state of  $2.13 \text{ D}$  [38] and the large polarizability of  $\sim 12 \text{ \AA}^3$  [39] suggests that it is potentially a major contributor for

solvating the adjacent charge, so that distortion of the polypeptide backbone induced by the charge is decreased. Pi-cation interactions are well-documented [40] and preliminary molecular dynamics simulations indicate that the Trp and Arg side chains can approach each other to within  $\leq 5$  Å (to be presented elsewhere). This interaction between Trp and the charge may also increase the fluorescence through reduction of the local electric field, thus decreasing the perturbation of the dye. However, in the absence of Trp the curvature of the peptide would increase to enable the charge to be solvated by backbone functional groups, e.g., carbonyl oxygens. Such curvature as well as the reduced number of amino acids decreases the end-to-end separation and increases the intramolecular collision rate yielding lower fluorescence. The larger slopes in the presence of Trp (Table 1) suggest that the combined effects of Trp and charge–dye interactions produce a larger decrease in fluorescence with increasing temperature than charge–dye interactions alone. Since the solvation effects result from an interaction between the Trp and charge, the effects of Trp and the charge on the fluorescence will not be additive.

The dependence of fluorescence on chain length for Pro<sub>4</sub> and Pro<sub>10</sub> results from the combination of two dynamics: intrinsic inflexibility of polyproline chains and intramolecular collision rates. Although the Pro<sub>10</sub> fluorescence should be greater assuming a smaller collision rate for the larger dye–Trp/charge separation, apparently the larger fluctuations of curvature possible for Pro<sub>10</sub> decreases the distance sufficiently to reduce the fluorescence amplitude relative to Pro<sub>4</sub>. The smaller slope for Pro<sub>10</sub> relative to Pro<sub>4</sub> suggests that increasing the temperature produces greater changes in the flexibility of the smaller chain length. It is interesting to note that an apparent saturation of the Pro<sub>4</sub> variation occurs at higher temperatures as the fluorescence for Pro<sub>4</sub> and Pro<sub>10</sub> converge (Fig. 4a).

The intrinsically large flexibility of the (GlySer)<sub>*m*</sub> peptides simplifies the interpretation of the fluorescence variation with temperature. In this case, the shorter chain length is not constrained and results in a smaller dye–Trp/charge separations resulting in higher collision rates. Trajectories of the longer chain explore a significantly larger phase space and so reduce the collision rate. The relative slopes of (GlySer)<sub>2</sub> and (GlySer)<sub>5</sub> indicate that increased temperature has a slightly greater effect on the longer chain as the same phase space is traversed more rapidly.

#### 4.3.2. 2+ Charge state

The most important change in the peptide dynamics for the 2+ charge state derives from the presence of Coulomb repulsion. Because the first charge is on the C-terminal Arg residue, the most probable position for the second charge is near the N-terminal residue to minimize the Coulomb repulsion. Although the repulsive force will tend to reduce the flexibility of peptide chains, increasing temperature continues to decrease the fluorescence but the rates of change are different for the 1+ and 2+ charge states (Table 1).

The fluorescence intensities of the 2+ ions at lower temperatures are reduced relative to those of the 1+ ions by  $\sim 25\%$  for Pro<sub>10</sub>,  $\sim 54\%$  for Pro<sub>4</sub> and  $\sim 64\%$  for (GlySer)<sub>*m*</sub> indepen-

Table 2  
Relative slopes of intensity vs. temperature of peptides in solution<sup>a</sup>

Peptide	Relative slope <sup>b</sup> (arb units K <sup>-1</sup> × 10 <sup>-3</sup> )
Pro <sub>10</sub>	-1.5 ± 0.2
Pro <sub>4</sub>	-4.6 ± 0.2
(GlySer) <sub>5</sub>	-4.7 ± 0.2
(GlySer) <sub>2</sub>	-8.2 ± 0.3

<sup>a</sup> Fit uncertainties are ± one standard deviation.

<sup>b</sup> Slope of the best-fit line.

dent of whether Trp is present. This suggests that the nearby charge dominates the reduction in fluorescence. As the temperature increases, so does the frequency of backbone fluctuations which result in dye–Trp and dye–charge interactions which reduce fluorescence. However, the Coulomb repulsion continues to constrain flexibility, depending on the peptide, which results in generally smaller slopes for the 2+ state than for the 1+ state.

#### 4.4. Solution measurements

Measurements of Pro<sub>*n*</sub> and (GlySer)<sub>*m*</sub> fluorescence as a function of temperature were performed in aqueous solution at pH 7 for comparison with the results obtained in gas phase. Clearly, the diffusion-limited kinetics will reduce collision rates but perhaps a more significant difference will be the shielding of charges by solvent. As a result, the dominant effects determining the slopes of fluorescence versus temperature will be the dye–Trp collisions depending on chain length and the relative peptide flexibility. The slopes provide a more reliable measure of the peptide dynamics than the absolute fluorescence intensities because they are unaffected by discrepancies in peptide concentration. The relative slopes of fluorescence versus temperature are shown in Table 2. The slope of the shorter chain length (*n* = 4 and *m* = 2) is greater than that of the longer chain length (*n* = 10 and *m* = 5) by a factor of 3 for Pro<sub>*n*</sub> and a factor of 1.7 for (GlySer)<sub>*m*</sub>. This is consistent with increased collision rates for the shorter dye–Trp separations. The (GlySer)<sub>2</sub> ((GlySer)<sub>5</sub>) slope is also greater than that of Pro<sub>4</sub> (Pro<sub>10</sub>) by a factor of 1.8 (3.1) due to the lower flexibility of poly(Pro) chains. The relative slopes measured in solution are a factor of  $\sim 100$  smaller than the relative slopes measured in gas phase, reflecting the reduced collision rates incurred by the diffusion-limited kinetics. A more detailed discussion of these solution fluorescence data and their comparison with fluorescence lifetime measurements are beyond the scope of this paper and will be presented elsewhere.

## 5. Conclusions

These measurements on peptides have identified interactions of an attached dye with a Trp residue and also with charged residues as the basis for variations of the fluorescence intensity. The Trp interaction leads to a quenching, non-radiative relaxation channel associated with a charge transfer process occurring within the collision complex. However, the dye interaction with a charged residue most likely perturbs the electronic levels of

the dye leading to shifts of the emission and excitation bands. Although this is not a quenching process, it does result in fluorescence changes. Measurements of either the lifetime or the dispersed spectrum in gas phase will allow fluorescence changes due to quenching and charge interactions to be determined independently. It should also be pointed out that having two processes to apply that are dependent on local interactions greatly increases the utility of these fluorescence techniques. However, in cases for which a Trp residue is not involved, it will be an advantage to be able to identify the most probable charge sites.

Fluorescence changes induced by local interactions in rather simple peptide chains have been shown to reflect a wide array of dynamical processes associated with changes in structure including the effects of Coulomb repulsion, backbone flexibility and charge-induced structure. The sensitivity of these measurements to local interactions, combined with judicious selection of peptide sequences and charge states for study, allows the individual effects to be identified. The power of this technique for studying conformational dynamics was demonstrated previously through measurements of conformational change in the Trp-cage protein [13], however, the extension of such studies to an arbitrary protein or peptide will require careful positioning of the dye and the Trp or charged residues to uniquely associate the change in fluorescence with a specific structural change.

The invaluable comparisons of the dynamical variations in solution with those measured in gas phase indicate significant differences between solution and gas phase dynamics stemming from shielding of charges by solvent and kinetic limits of diffusion. Molecular dynamics simulations currently in progress will be particularly valuable for elucidating the details of the conformational changes induced by temperature and the relationship between collision processes and biomolecular structure.

## Acknowledgments

The authors thank Abraham Szöke, Evan Williams and Thomas Rizzo for useful discussions and reviewers for identifying research related to these studies. This work was supported by the Rowland Institute at Harvard.

## References

- [1] T. Wyttenbach, G. von Helden, M.T. Bowers, *J. Am. Chem. Soc.* 118 (1996) 8355.
- [2] R.R. Hudgins, M.F. Jarrold, *J. Am. Chem. Soc.* 121 (1999) 3494.
- [3] M.F. Jarrold, *Ann. Rev. Phys. Chem.* 51 (2000) 179.
- [4] E.R. Badman, S. Myung, D.E. Clemmer, *J. Am. Soc. Mass Spectrom.* 16 (2005) 1493.
- [5] X. Cheng, C. Fenselau, *Int. J. Mass Spectrom. Ion Processes* 122 (1992) 109.
- [6] S. Campbell, M.T. Rodgers, E.M. Marzluff, J.L. Beauchamp, *J. Am. Chem. Soc.* 117 (1995) 12840.
- [7] M.K. Green, C.B. Lebrilla, *Mass Spectrom. Rev.* 16 (1997) 53.
- [8] P.D. Schnier, W.D. Price, R.A. Jockusch, E.R. Williams, *J. Am. Chem. Soc.* 118 (1996) 7178.
- [9] H. Oh, K. Breuker, S.K. Sze, Y. Ge, B.K. Carpenter, F.W. McLafferty, *Proc. Natl. Acad. Sci. U.S.A.* 99 (2002) 15863.
- [10] C.M. Adams, F. Kjeldsen, R.A. Zubarev, B.A. Budnik, K.F. Haselmann, *J. Am. Soc. Mass Spectrom.* 15 (2004) 1087.
- [11] N.C. Polfer, K.F. Haselmann, P.R.R. Langridge-Smith, P.E. Barran, *Mol. Phys.* 103 (2005) 1481.
- [12] J. Oomens, N. Polfer, D.T. Moore, L. van der Meer, A.G. Marshall, J.R. Eyler, G. Meijer, G. von Helden, *Phys. Chem. Chem. Phys.* 7 (2005) 1345.
- [13] A.T. Iavarone, J.H. Parks, *J. Am. Chem. Soc.* 127 (2005) 8606.
- [14] L.J. Lapidus, W.A. Eaton, J. Hofrichter, *Proc. Natl. Acad. Sci. U.S.A.* 97 (2000) 7220.
- [15] R.R. Hudgins, F. Huang, G. Gramlich, W.M. Nau, *J. Am. Chem. Soc.* 124 (2002) 556.
- [16] N. Marmé, J.-P. Knemeyer, M. Sauer, J. Wolfrum, *Bioconjugate Chem.* 14 (2003) 1133.
- [17] F. Huang, R.R. Hudgins, W.M. Nau, *J. Am. Chem. Soc.* 126 (2004) 16665.
- [18] A.C. Vaiana, H. Neuweiler, A. Schulz, J. Wolfrum, M. Sauer, J.C. Smith, *J. Am. Chem. Soc.* 125 (2003) 14564.
- [19] S.J. Hagen, C.W. Carswell, E.M. Sjolander, *J. Mol. Biol.* 305 (2001) 1161.
- [20] S.A. Pabit, H. Roder, S.J. Hagen, *Biochemistry* 43 (2004) 12532.
- [21] H. Neuweiler, A. Schulz, M. Böhmer, J. Enderlein, M. Sauer, *J. Am. Chem. Soc.* 125 (2003) 5324.
- [22] O. Bieri, J. Wirz, B. Hellrung, M. Schutkowski, M. Drewello, T. Kiefhaber, *Proc. Natl. Acad. Sci. U.S.A.* 96 (1999) 9597.
- [23] <http://probes.invitrogen.com>.
- [24] A.S. Danell, J.H. Parks, *Int. J. Mass Spectrom.* 229 (2003) 35.
- [25] J.T. Khoury, S.E. Rodriguez-Cruz, J.H. Parks, *J. Am. Soc. Mass Spectrom.* 13 (2002) 696.
- [26] M. Wilm, M. Mann, *Anal. Chem.* 68 (1996) 1.
- [27] G. Jones, L. Lu, V. Vullev, D.J. Gosztola, S.R. Greenfield, M.R. Wasielewski, *Bioorg. Med. Chem. Lett.* 5 (1995) 2385.
- [28] G. Jones, Z. Xin, V.I. Vullev, *Photochem. Photobiol. Sci.* 2 (2003) 1080.
- [29] C.C. Moser, J.M. Keske, K. Warncke, R.S. Farid, P.L. Dutton, *Nature* 355 (1992) 796.
- [30] H. Yang, G. Luo, P. Karnchanaphanurach, T.-M. Louie, I. Rech, S. Cova, L. Xun, X.S. Xie, *Science* 302 (2003) 262.
- [31] M.D. Newton, in: J. Jortner, M. Bixon (Eds.), *Electron Transfer—From Isolated Molecules to Biomolecules, Part 1*, Wiley, New York, 1999, p. 310.
- [32] B. Kuhn, P. Fromherz, W. Denk, *Biophys. J.* 87 (2004) 631.
- [33] O. Kwame, A. Joseph, P. Wuskell, L.M. Loew, F. Bezanilla, *Neuron* 37 (2003) 85.
- [34] M. Sczegan, W. Rettig, A.I. Tolmachev, *Photochem. Photobiol. Sci.* 2 (2003) 1264.
- [35] H. Kang, C. Jouvet, C. Dedonder-Lardeux, S. Martrenchard, G. Grégoire, C. Desfrancois, J.-P. Schermann, M. Barat, J.A. Fayeton, *Phys. Chem. Chem. Phys.* 7 (2005) 394.
- [36] F. Bergström, I. Mikhalyov, P. Hägglöf, R. Wortmann, T. Ny, L.B.-Å. Johansson, *J. Am. Chem. Soc.* 124 (2002) 196.
- [37] E.V. Tsiper, Z.G. Soos, *Phys. Rev. B* 64 (2001) 195124.
- [38] A.L. McClellan, *Tables of Experimental Dipole Moments*, Freeman, London, 1963.
- [39] I. Compagnon, F.C. Hagemeister, R. Antoine, D. Rayane, M. Broyer, P. Dugourd, R.R. Hudgins, M.F. Jarrold, *J. Am. Chem. Soc.* 123 (2001) 8440.
- [40] J.P. Gullivan, D.A. Dougherty, *J. Am. Chem. Soc.* 122 (2000) 870.